Scattering of a two skyrmion configuration on potential holes or barriers in a model Landau–Lifshitz equation

2009 J. Phys. A: Math. Theor. 42 165102

(http://iopscience.iop.org/1751-8121/42/16/165102)

IOP PUBLISHING JOURNAL OF PHYSICS A: MATHEMATICAL AND THEORETICAL

J. Phys. A: Math. Theor. **42** (2009) 165102 (18pp) doi:10.1088/1751-8113/42/16/165102

Scattering of a two skyrmion configuration on potential holes or barriers in a model Landau–Lifshitz equation

J C Collins and W J Zakrzewski

Department of Mathematical Sciences, University of Durham, Durham DH1 3LE, UK

E-mail: J.C.Collins@durham.ac.uk and W.J.Zakrzewski@durham.ac.uk

Received 17 October 2008, in final form 5 March 2009
Published 31 March 2009
Online at stacks.iop.org/JPhysA/42/165102

Abstract

The dynamics of a baby-skyrmion configuration, in a model Landau–Lifshitz equation, was studied in the presence of various potential obstructions. The baby-skyrmion configuration was constructed from two $Q = 1$ hedgehog solutions to the baby-skyrme model in (2+1) dimensions. The potential obstructions were created by introducing a new term into the Lagrangian which resulted in a localized inhomogeneity in the potential terms' coefficient. In the barrier system, the normal circular path was deformed as the skyrmions traversed the barrier. During the same period, it was seen that the skyrmions sped up as they went over the barrier. For critical values of the barrier height and width, the skyrmions were no longer bound and were free to separate. In the case of a potential hole, the baby skyrmions no longer formed a bound state and moved asymptotically along the axis of the hole. It is shown how to modify the definition of the angular momentum to include the effects of the obstructions, so that it is conserved.

PACS numbers: 12.39.Dc, 11.10.Lm, 75.10.Hk

1. Introduction

The scattering of particles off potential holes and barriers in classical and quantum mechanical systems is seemingly different. In a classical system, if the particle has sufficient energy it can traverse a barrier; if it does not, it gets reflected. When it encounters a hole it speeds up as it passes over the hole and is always transmitted. In both cases the particle is either transmitted or reflected. In quantum mechanical scattering the particle can be reflected and transmitted for either a barrier or a hole but these events occur with a certain probability which is dependent on the particle's energy and on the size of the barrier or the hole.

In this paper, we examine the scattering properties of a topological soliton in magnetic systems, whose motion is then governed by the Landau–Lifshitz equation. Topological solitons are, of course, classical objects (as they satisfy classical equations of motions). However, they describe extended objects and, as shown in [1], some of their properties resemble those of quantum systems. Hence, in this paper we study this problem further, this time concentrating on systems whose dynamics is described by a Landau–Lifshitz equation. This equation arises in the dynamics of magnetic bubbles and so, in this paper, we look at the behaviour of topological solitons in the presence of potential obstructions. The topological solitons under investigation are baby skyrmions which are thought to describe the experimentally observable magnetic bubbles.

Our investigation should also shed some light on the properties of magnetic bubbles. Such bubbles are not mathematical artefacts but have been produced experimentally by subjecting a ferromagnetic material to a pulsed magnetic field. The ferromagnetic domains of the material are then squeezed by the field. If a field of large enough magnitude is applied over a sufficient length of time, the magnetic domains of the system collapse leaving behind the material which is uniformly magnetized in the direction of the applied field. This process is not instantaneous or uniform. As the domains tend to align with the applied field, the pulsing of certain materials results in the pinching of the domain walls into a cylindrical domain called a magnetic bubble. Magnetic bubbles were once considered as an alternative form of memory storage due to the density at which they could be stored.

In real three-dimensional systems the magnetic bubbles are stabilized by the finite thickness of the thin films in which they are created. The model examined here is strictly in 2D. In this case the bubbles are stabilized by the introduction of the slightly artificial skyrme term. For more realistic calculations one would need to perform 3D simulations. Magnetic bubbles and their properties have been extensively experimentally researched; further information on this research can be found in [3, 4].

The baby-skyrme model in (2+1) dimensions is defined by

$$\mathcal{L} = \tfrac{1}{2}\gamma_1 \partial_\mu \underline{\phi} \cdot \partial^\mu \underline{\phi} - \tfrac{1}{4}\gamma_2[(\partial_\mu \underline{\phi} \cdot \partial^\mu \underline{\phi})^2 - (\partial_\mu \underline{\phi} \cdot \partial_\nu \underline{\phi})(\partial^\mu \underline{\phi} \cdot \partial^\nu \underline{\phi})] - V(\underline{\phi}), \tag{1}$$

where $\underline{\phi}$ is a three-component scalar field and the indices run over the spacetime coordinates. This is referred to as the baby-skyrme model to distinguish it from the full skyrme nuclear model of baryons. The first term is the exchange energy, the second and third terms are the skyrme term and the potential term, respectively. The latter two terms have been introduced to avoid the consequences of Derrick's theorem [5] and to stabilize topological soliton solutions in two dimensions. The condition that $\underline{\phi}^2 = 1$ is imposed so that the target space is the 2-sphere, such that $\underline{\phi}$ is now a map $\underline{\phi} : \mathbb{R}^2 \to S^2$. For finite energy solutions it is necessary for the fields to tend to a vacuum at infinity, where $\phi_3 = 1$ at ∞. This results in a compactification of $\mathbb{R}^2$ so that $\underline{\phi}$ now takes values in the extended plane $\mathbb{R}^2 \cup \infty$, which is topologically equivalent to S^2. The constraint equation $\underline{\phi}^2 = 1$ and the boundary condition at infinity results in the field $\underline{\phi}$ becoming a non-trivial map $\underline{\phi} : S^2 \to S^2$. Each soliton solution is grouped into a different homotopy class according to the winding number, or topological charge, of this map. The topological charge Q is given by

$$Q = \frac{1}{8\pi} \int_{-\infty}^{\infty} \epsilon_{ij} \underline{\phi} \cdot (\partial_j \underline{\phi} \times \partial_i \underline{\phi}) \, \mathrm{d}^2 x, \tag{2}$$

where the indices i, j run over the space coordinates and $Q \in \mathbb{Z}$. The topological soliton solutions of the baby-skyrme model are called baby skyrmions. Here, for simplicity, we shall refer to baby skyrmions of charge Q as Q-skyrmions. Recent work has shown that the continuum dynamical equation in anti-ferromagnetic systems also resembles a second-order

relativistic wave equation [2] in which such soliton solutions exist. The work in [2] established many interesting properties of solitons in such systems.

Our discussion so far has concerned the relativistic systems of skyrmions. However, as we said above, they also arise in the description of magnetic bubbles, but this time their evolution is described by the first-order Landau–Lifshitz equation. The Landau–Lifshitz equation is given by

$$\frac{\partial \underline{\phi}}{\partial t} = \underline{\phi} \times \frac{-\delta W}{\delta \underline{\phi}}, \tag{3}$$

where W is the energy functional written as

$$W = \int\int_{-\infty}^{\infty} w \, \mathrm{d}x \, \mathrm{d}y, \tag{4}$$

and w is the static part of (1) given by

$$w = \tfrac{1}{2}\gamma_1 \partial_i \underline{\phi} \cdot \partial_i \underline{\phi} + \tfrac{1}{4}\gamma_2[(\partial_i \underline{\phi} \cdot \partial_i \underline{\phi})^2 - (\partial_i \underline{\phi} \cdot \partial_j \underline{\phi})(\partial_i \underline{\phi} \cdot \partial_j \underline{\phi})] + V(\underline{\phi}).$$

Thus we can write $\frac{\delta W}{\delta \underline{\phi}}$:

$$\frac{\delta W}{\delta \underline{\phi}} = \gamma_1 \nabla^2 \underline{\phi} - \frac{\partial V(\underline{\phi})}{\partial \underline{\phi}} + \frac{1}{2}\gamma_2\{2\partial_i[(\partial_j \underline{\phi} \cdot \partial_j \underline{\phi})\partial_i \underline{\phi}] - \partial_i[(\partial_i \underline{\phi} \cdot \partial_j \underline{\phi})\partial_j \underline{\phi}] - \partial_j[(\partial_i \underline{\phi} \cdot \partial_j \underline{\phi})\partial_i \underline{\phi}]\}.$$

Analysis of the dynamics in Landau–Lifshitz systems has been greatly simplified by the work of Papanicolaou and Tomaras [10], who constructed unambiguous conservation laws for the system governed by (3). In their work they found that the important quantity was the topological charge density q:

$$q = \epsilon_{ij} \underline{\phi} \cdot (\partial_j \underline{\phi} \times \partial_i \underline{\phi}). \tag{5}$$

Some of the conservation laws can be constructed as a moment of q. They involve

$$l = \frac{1}{2}\int\int_{-\infty}^{\infty} \underline{x}^2 q \, \mathrm{d}x \, \mathrm{d}y, \tag{6}$$

$$m = \int\int_{-\infty}^{\infty} (\phi_3 - 1) \, \mathrm{d}x \, \mathrm{d}y, \tag{7}$$

$$J = l + m, \tag{8}$$

where l is the orbital angular momentum, m is the total magnetization in the third direction and J is the total angular momentum. Conservation laws for the system were constructed by examining the time evolution of q:

$$\dot{q} = -\epsilon_{ij} \partial_i \partial_l \sigma_{jl}, \tag{9}$$

where $\partial_l \sigma_{jl}$ can be written in terms of the energy functional W:

$$\partial_l \sigma_{jl} = \left(\frac{\delta W}{\delta \underline{\phi}} \cdot \partial_j \underline{\phi} \right). \tag{10}$$

Taking an explicit time derivative of (1) gives

$$\dot{l} = \frac{1}{2}\int\int_{-\infty}^{\infty} \underline{x}^2 \dot{q} \, \mathrm{d}x \, \mathrm{d}y, \tag{11}$$

and we note that this can be recast as

$$\dot{l} = \iint_{-\infty}^{\infty} \epsilon_{ij}\sigma_{ij}\,\mathrm{d}x\,\mathrm{d}y \tag{12}$$

by integrating (11) by parts. In the case of a system with a symmetric tensor σ_{ij}, $\dot{l} = 0$ and angular momentum is conserved.

The guiding centre coordinate $\underline{R}$ of the soliton is defined as the first moment of the topological charge density q:

$$\underline{R} = \frac{1}{4\pi Q}\iint_{-\infty}^{\infty} \underline{x}q\,\mathrm{d}x\,\mathrm{d}y. \tag{13}$$

Since our solitons are in two spatial dimensions, their position can generally be defined as the location of the centre of each soliton. This definition can be interpreted in two ways. One can consider the soliton centre to be the point at which the third component of the field $\phi_3 = -1$ or to be the maxima of the topological charge density q. It was seen in previous simulations [8] that both of these definitions produce near identical trajectories. One can also consider the mean squared radius r of the solitons, defined by

$$r^2 = \frac{1}{4\pi Q}\iint_{-\infty}^{\infty} (\underline{x} - \underline{R})^2 q\,\mathrm{d}x\,\mathrm{d}y. \tag{14}$$

One can expand out (14) to find a relationship between the mean squared radius of the solitons and l:

$$r^2 = \frac{l}{2\pi Q} - \underline{R}^2. \tag{15}$$

This relationship among l, r and R greatly helps to understands the dynamics described in later sections.

Much of the previous work on baby-skyrme models, in the context of Landau–Lifshitz dynamics, has concerned the choice of two different potential terms $V(\phi)$:

$$V(\phi) = \tfrac{1}{2}\gamma_3(1 - \phi_3)^4, \tag{16}$$

$$V(\phi) = \tfrac{1}{2}\gamma_3(1 - {\phi_3}^2). \tag{17}$$

Models which employ either of these potentials are commonly referred to as the holomorphic baby-skyrme model (16) and the 'new' baby-skyrme model (17) to distinguish it from the holomorphic one. The holomorphic model was first studied in the context of Landau–Lifshitz dynamics in [8], since it provided an analytical solution to the system of equations. The topological solitons of this model are polynomially localized. In [8] it was shown that two 1-skyrmions orbited around each other along deformed circular trajectories. Their work involved a local magneto-static field in addition to the three previous terms in (1), which resulted in the non-conservation of l and m. The total angular momentum J was well conserved in time. The authors of [8] attributed the non-conservation of l and m to the non-symmetric structure of σ_{jl} due to the presence of the magneto-static field.

The new baby-skyrme model is a more realistic case of easy axis anisotropy and we use this in our study, i.e. we consider $V(\phi)$ to take the form of (17). Some of the work done on it has been in relation to the dynamics of magnetic bubbles [7]; this study also involved a local magneto-static field. Analytic solutions do not exist and so all solutions must be found numerically. The topological solitons of this model are exponentially localized. In [7] it was found that two $Q = 1$-skyrmions orbited each other on a circular trajectory modified by a Larmor procession due to the magnetic field. J was well conserved in time but its constituent

components l and m were not. The arguments for the non-conservation were identical to those in the holomorphic model. Since those early papers, there has been extensive work done on both these models and their multi-skyrmion structures. The details can be found in the work of Weidig [6] or for a larger class of potentials $V(\underline{\phi})$ in [9].

2. Constructing the initial field configuration

Seeking a static field configuration which is a solution of (3) for a potential term $V(\phi)$ of the form (17), we assume that the solitons take the form of a hedgehog configuration for a Q-skyrmion:

$$\phi = (\cos(Q\theta)\sin(f(r)), \sin(Q\theta)\sin(f(r)), \cos(f(r))), \tag{18}$$

where $f(r)$ is the profile function satisfying certain boundary conditions, θ is the polar angle and Q is the topological charge of the skyrmions. The skyrmion solutions are minima of the energy functional (4). We are interested in the dynamics of $Q = 1$ skyrmions. Inserting the hedgehog configuration for $Q = 1$ into the energy functional and minimizing the integral result in a second-order differential equation for the profile function $f(r)$:

$$f''\left(\gamma_1 r + \frac{\gamma_2 \sin^2 f}{r}\right) + f'\left(\gamma_1 - \frac{\gamma_2 \sin^2 f}{r^2}\right) + f'^2\left(\frac{\gamma_2 \sin f \cos f}{r}\right) - \frac{\gamma_1 \sin f \cos f}{r} - \gamma_3 r \cos f \sin f = 0. \tag{19}$$

This can be rearranged into the form $f'' = h(r, f, f')$. The profile function must satisfy certain boundary conditions for there to exist finite energy solutions. The boundary conditions impose constraints on $f(r)$ at the origin and infinity: $f(0) = \pi$ and $f(\infty) = 0$. The second-order differential equation for $f(r)$ can be solved numerically using the shooting method. With the profile function obtained we can construct from (18) a 1-skyrmion solution to (3). A two 1-skyrmion configuration can be constructed by the superposition procedure. The easiest method to do this is to transform the fields to a stereographic variable Ω:

$$\begin{aligned}
\Omega &= \frac{\phi_1 + \mathrm{i}\phi_2}{1 + \phi_3}, \\
\phi_1 &= \frac{\Omega + \Omega^*}{1 + |\Omega|^2}, \\
\phi_2 &= \frac{1}{\mathrm{i}} \frac{\Omega - \Omega^*}{1 + |\Omega|^2}, \\
\phi_3 &= \frac{1 - |\Omega|^2}{1 + |\Omega|^2}.
\end{aligned} \tag{20}$$

The stereographic variable Ω can then be rewritten in terms of the hedgehog ansatz variables, $f(r)$ and θ, as

$$\Omega = \tan\left(\frac{f(r)}{2}\right) \mathrm{e}^{\mathrm{i}\theta}.$$

To construct a two $Q = 1$-skyrmion configuration in which the two skyrmions are in an attractive channel, we take

$$\begin{aligned}
\Omega &= \Omega_1 - \Omega_2, \\
\Omega_1 &= \tan\left(\frac{f(r_1)}{2}\right) \mathrm{e}^{\mathrm{i}\theta_1}, \\
\Omega_2 &= \tan\left(\frac{f(r_2)}{2}\right) \mathrm{e}^{\mathrm{i}\theta_2},
\end{aligned} \tag{21}$$

where $r_i = \sqrt{((x-x_i)^2+(y-y_i)^2)}$ and $\theta_i = \tan^{-1}\left(\frac{y-y_i}{x-x_i}\right)$ are calculated relative to the centres of the skyrmions (x_i, y_i). During the simulations it was found that the configuration constructed in this manner did not replicate the skyrmion ring configurations for small values of $d = \sqrt{((x_1-x_2)^2+(y_1-y_2)^2)}$; see [6]. The superposition procedure was a very good approximation to a two 1-skyrmion configuration for values of $d > 6$, where the skyrmions were well separated to be distinct. To obtain a true representation of the configuration for all values of d, we used a gradient flow method to 'relax' the field configuration. The above field configuration (21) constructed for skyrmion separation $d = 8$ was used as an initial condition of the gradient flow equation given by

$$\frac{\partial \underline{\phi}}{\partial t} = -\kappa \frac{\delta W}{\delta \underline{\phi}} + k\underline{\phi},$$

where k is a Lagrange multiplier introduced such that the constraint $\underline{\phi}^2 = 1$ is satisfied. The field configurations obtained by this relaxation method show the required ring-like properties for small values of the skyrmion separation.

3. Potential obstruction

In this paper, we study the scattering properties of a two $Q = 1$-skyrmion configuration on a potential obstruction which is localized in a finite region of space. In constructing the obstruction we adopt a similar approach used in the previous work of one of the authors [1] and introduce a term into the Lagrangian (1) which vanishes in the vacuum state $\phi_3 = +1$. The obstructions need to be introduced in this way so that the tails of the solitons are not changed by the obstruction. Therefore, we add the additional potential term $V_{\text{obstruction}}(\phi_3)$ which is identical to the potential in (1) and is localized to a finite region of space:

$$\mathcal{L}_{\text{new}} = \mathcal{L}_{\text{old}} + V_{\text{obstruction}}(\phi_3),$$

where

$$V_{\text{obstruction}}(\phi) = \tfrac{1}{2}\Gamma\left(1-\phi_3^2\right). \tag{22}$$

Γ can be either positive or negative. The Lagrangian of (1), by the introduction of this additional potential, is changed such that the potential coefficient now depends on the space coordinates. The introduction of this term implies that the static part of (1) can be rewritten as

$$\mathcal{L} = \tfrac{1}{2}\gamma_1 \partial_i \underline{\phi} \cdot \partial_i \underline{\phi} - \tfrac{1}{4}\gamma_2[(\partial_i \underline{\phi} \cdot \partial_i \underline{\phi})^2 - (\partial_i \underline{\phi} \cdot \partial_j \underline{\phi})(\partial_i \underline{\phi} \cdot \partial_j \underline{\phi})] - \tfrac{1}{2}\gamma_3(x,y)\left(1-\phi_3^2\right), \tag{23}$$

where the potential term coefficient γ_3 is now a function of the coordinates (x, y) and the static part of (1) is only considered as imposed by the Landau–Lifshitz equation (3). This inhomogeneity will be localized to a finite region of space. The sign of Γ determines whether the potential obstruction is a hole or a barrier. When $\Gamma > 0$, the obstruction is a barrier. Conversely, when $\Gamma < 0$ the obstruction is a hole.

4. Numerical procedures and the free system dynamics

Unfortunately, it is impossible to solve (3) analytically, we have therefore had to study this problem numerically. The fields and their derivatives were discretized in the usual manner and were placed on a lattice of 251×251 points, with lattice spacing $\mathrm{d}x = 0.1$. The numerical integration of the three-coupled differential equations of (3) involved the use of a fourth-order Runge–Kutta method of simulating time evolution with a time step of $\mathrm{d}t = 0.001$. The various integrals calculated throughout the simulations were performed using a 2D Simpson's

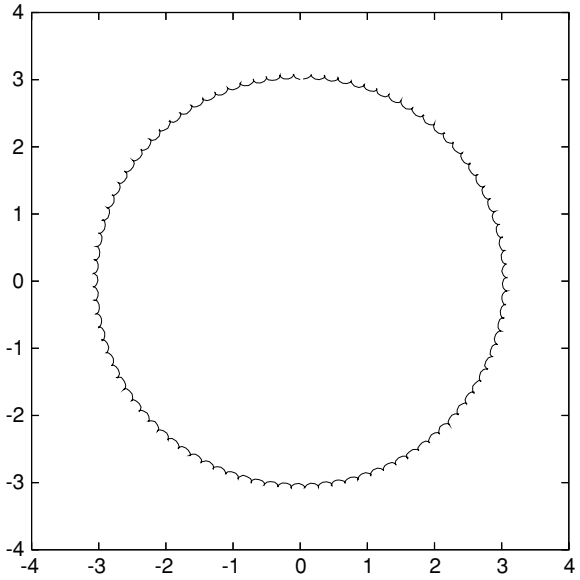

Figure 1. Trajectory of the upper skyrmion in the absence of any obstruction for a two 1-skyrmion configuration.

rule. The constraint equation requires that the fields lie on the 2-sphere, $\underline{\phi}^2 = 1$, and this was imposed at every time step by rescaling each field component so that $\phi_i \to \frac{\phi_i}{\sqrt{\underline{\phi}\cdot\underline{\phi}}}$.

The skyrmions were initially placed at $(0, \pm d/2)$ in the upper and lower planes, where d is the distance between the two skyrmion centres (x_i, y_i). The trajectory of each skyrmion was tracked by following the maxima of the topological charge density and interpolating between the lattice points. All of the simulations have been performed for a skyrmion separation of $d = 6$. This was found to be the optimum distance, where the skyrmions are separated enough from each other to be distinct but close enough to interact. The coefficients γ_i have been set to unity in all the simulations unless stated otherwise.

4.1. No obstruction dynamics

Initially we examined the behaviour of the skyrmions without an obstruction, i.e. with $\Gamma = 0$. Figure 1 shows the trajectory of the upper skyrmion of a two 1-skyrmion configuration for $\Gamma = 0$. The skyrmions orbit around the configuration's centre $(0, 0)$. The trajectories of each skyrmion lie along a circle of radius $r \simeq 3$. Their position undergoes mild oscillations during the simulation. The total energy E_{tot} and angular momentum $J = l + m$ are conserved with time. Additionally, each individual angular momentum component l and m is also conserved. The timescale for one period is 700 s. This motion of two baby skyrmions in a Landau–Lifshitz system is well understood and an analogy with the Hall motion of two interacting electrons is usually invoked when discussing their trajectory [10].

5. Simple obstruction

There are many choices one can make for the geometry of the potential obstruction. The simplest choice initially studied was a symmetric obstruction. The obstruction was placed

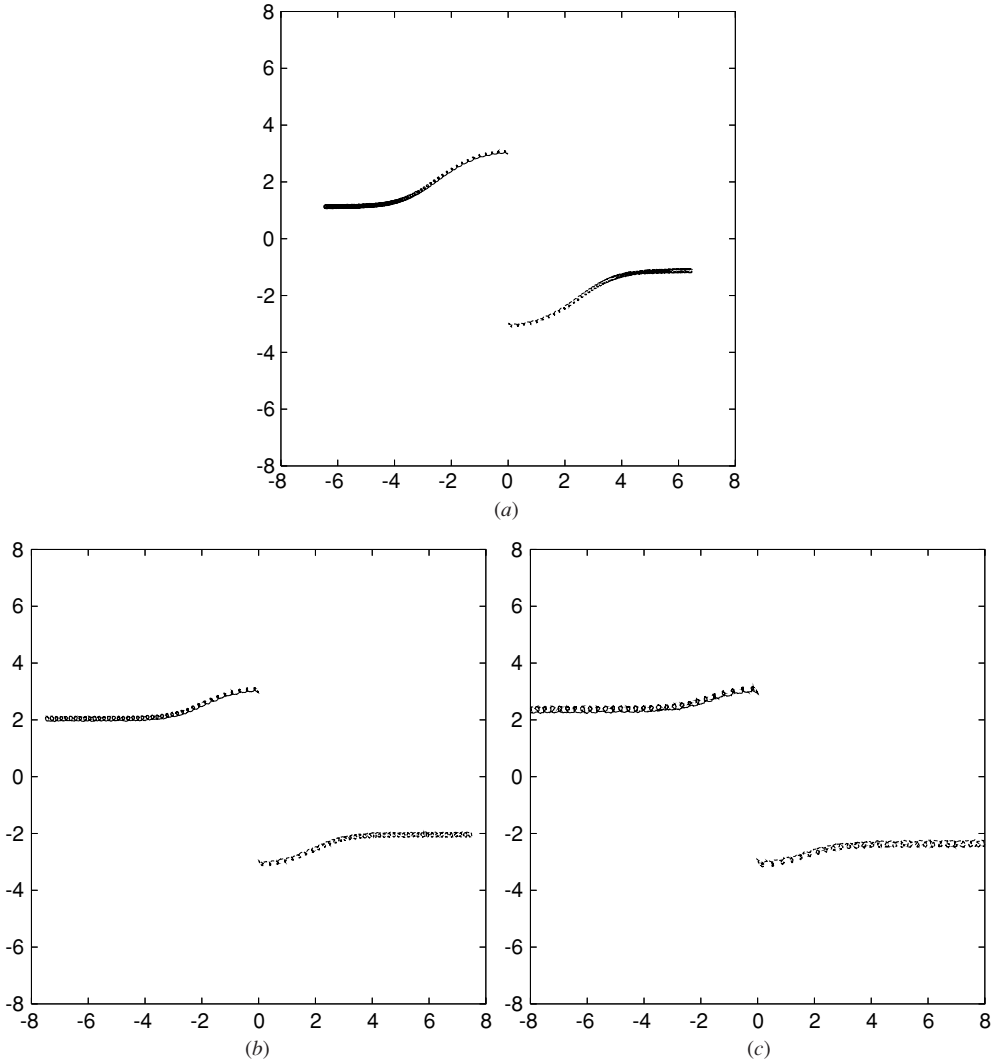

Figure 2. Trajectories for both the upper and lower skyrmions with a potential hole, for $b = 1$ and with the time length shown in brackets: (*a*) $\Gamma = -0.1$ (690 s), (*b*) $\Gamma = -0.25$ (290 s) and (*c*) $\Gamma = -0.5$ (215 s).

symmetrically along the x-axis with width b, i.e. starting at $y = -b/2$ and continuing up to $y = b/2$ and extending for all values of x. In our study, we look at the differences of dynamics due to holes and barriers. They will be discussed in the following sections.

5.1. Potential hole

We start by recalling that in the absence of all obstructions the skyrmion executes a circular path around their centre. Figure 2 shows the trajectories of the upper and lower skyrmions encountering a potential hole for different values of Γ, for $b = 1$. In all plots the skyrmions initially try to execute the trajectory of figure 1 but are deflected. They move asymptotically

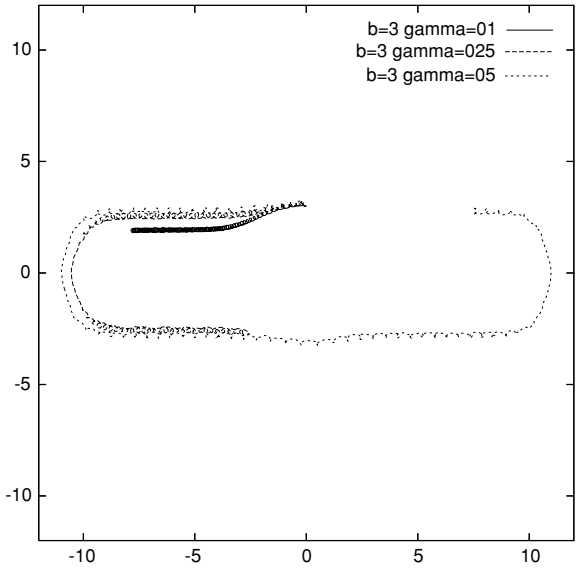

Figure 3. Plot of the trajectories of the upper skyrmion in a system with a potential hole of width $b = 3$ for various values of Γ.

along the axis of the hole at an approximately constant value, $y_{\max}$. It is clear from figure 2 that the larger the $|\Gamma|$, the larger the value of $y_{\max}$. The skyrmions of figure 2(a) are able to get 'closer' to the hole than the skyrmions of figure 2(b) or figure 2(c). Figure 3 shows the trajectories of only the upper skyrmions interacting with the potential hole for various values of Γ when b $= 3$. Comparing this plot with those in figure 2, one sees the effect of a larger b. The larger the b the larger the $y_{\max}$ for a given Γ. The skyrmions' tail can feel the hole earlier in a system of larger b than in a system of smaller b. The same dependence of $y_{\max}$ on Γ is evident in figure 3. In figure 3 the skyrmion trajectories of $\Gamma = -0.25, -0.5$ are seen to be reflected by the boundary. The skyrmions in the lower plane execute similar trajectories.

To explain the observed behaviour of skyrmions when encountering a hole, which may at first sight appear as non-classical, we need to examine the binding energies of the configuration. If the energy of the two 1-skyrmion configuration in the presence of a hole is denoted by E_2, and E_1 is the energy of a single 1-skyrmion placed at the same position as one of the skyrmions in E_2, then the binding, or the interaction energy, is given by

$$E_B = E_2 - 2E_1. \tag{24}$$

In the system with $b = 1, \Gamma = -0.25$ we have $E_2 = 2.1206/8\pi$ and $E_1 = 1.0685/8\pi$. The binding energy of the two skyrmions in this system is thus $E_B = -0.0174/8\pi$, which is negative. Thus initially the skyrmions behave as if they are still in a bound state, and try to execute the usual circular motion about their centre. If we examine the plot of the trajectory in figure 2, we see that as the skyrmions approach the hole, they reach a point where they separate and behave as two unbound skyrmions. Considering the definition of E_1, we can compute the energy of the single skyrmion as a function of the distance from the hole. Initially the skyrmion is at a distance $D = 3$ from the centre of the $b = 1$ hole and the binding energy is $E_B = -0.0174/8\pi$. If $D = 2$ the binding energy is reduced to $E_B = -0.005/8\pi$ and if the skyrmion is brought closer at $D = 1$ then $E_B = +0.0152/8\pi$. So, as the skyrmions approach the hole the binding energy of the configuration is modified such that they no longer

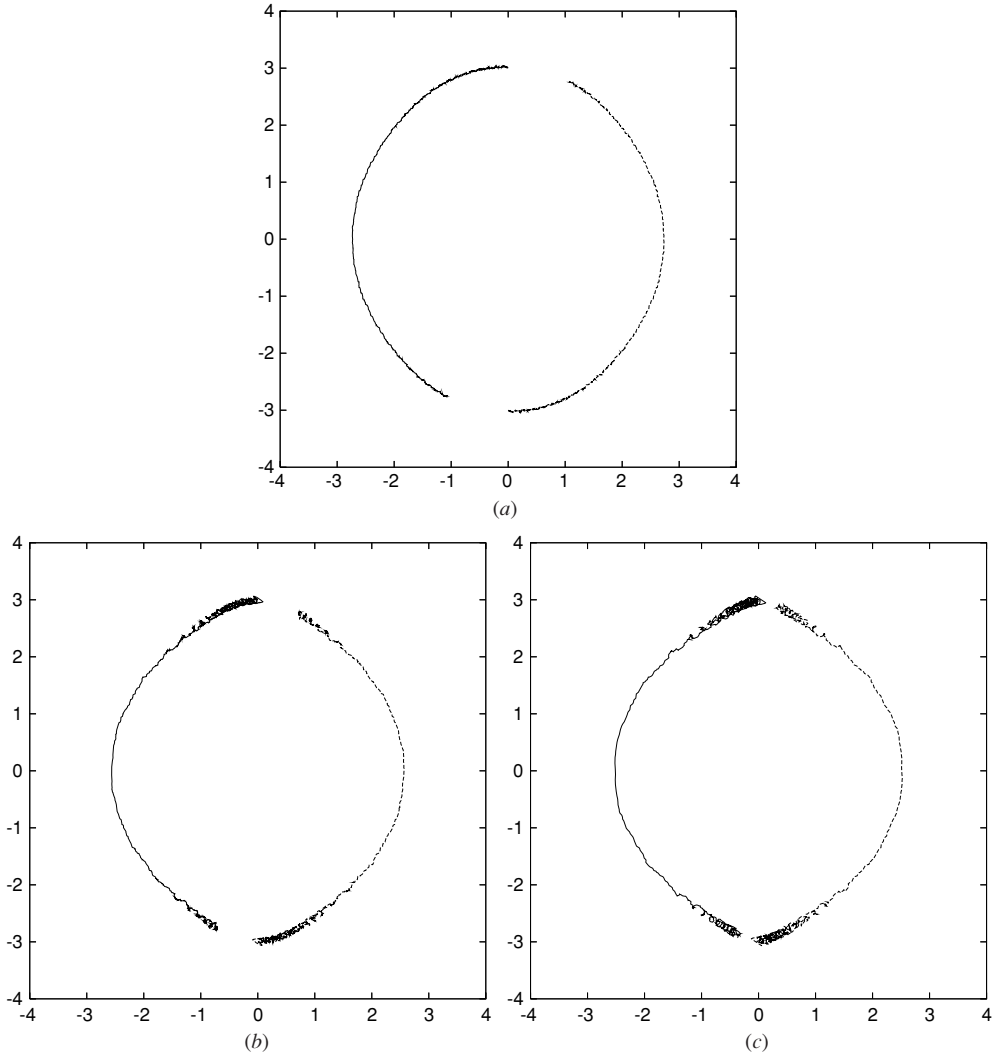

Figure 4. Trajectories of upper and lower skyrmions for the $b = 2$ barrier system for various values of Γ: (*a*) $\Gamma = 0.1$, (*b*) $\Gamma = 0.25$ and (*c*) $\Gamma = 0.3$.

form a bound state and are able to separate. It is clear from the plots of the trajectory that the skyrmions, for a smaller value of Γ, are able to get closer to the hole than those for larger values of Γ. The skyrmions are able to get closer in these systems, because the binding energies of the skyrmions do not reach its critical value until the skyrmions get closer to the hole. In the system of a larger value of Γ the hole modifies the binding energy earlier, and thus the system reaches its critical value before the skyrmions can get as close as those for the smaller Γ.

5.2. Potential barrier

Next, we have studied several cases of the scattering of the same two 1-skyrmion configuration off potential barriers. Figure 4 shows the trajectories of the upper and lower skyrmions of a two

1-skyrmion configuration scattering off a potential barrier of width $b = 2$, for various values of Γ. It can be seen in each plot that the skyrmions are deflected as they traverse the barrier. This deflection always occurs in the direction of the centre of the configuration and hence the normal circular path is deformed as the skyrmions overcome the barrier. Trajectories for a smaller barrier width show a sharper deflection than those with larger b. Since the skyrmions are extended objects, when they traverse the barrier they feel the barrier the most at the middle point. It is then only natural that the maximum point of deviation from the normal circular path will be at this point. Comparing trajectories of the same Γ but with different values of b, we note that the skyrmions in the system with the larger value of b have more time to adjust to the barrier once they are 'on' top of it and therefore their path is not as sharp as for a smaller b. The larger value of b 'smooths' out the sharpening effects seen in the system with a smaller value of bs. More interestingly, during this deviation the skyrmions speed up as they traverse the barrier. In figures 4(a) and (b) the times taken for the skyrmion centre to reach the edge of the barrier are 110 s and 140 s respectively, but the times taken for the centre to traverse the full width of the barrier are only 25 s and 12.5 s.

The deflection and speeding up of the skyrmions can be explained by remembering how the skyrmions are constructed. As explained in section 2, our two 1-skyrmion configuration was constructed in such a way that the skyrmions were in an attractive channel. When they encounter a barrier the energy of their configuration would have to increase. The skyrmions counteract this increase due to the barrier by reducing their separation distance d. This is clear by considering the energies of the configuration away from the barrier with $d = 6$. The energy of such a configuration is $E = 2.1277$. If the same configuration was then placed on the barrier with $\Gamma = 0.2$, the energy becomes $E = 2.1283$. Thus any increase in the potential energy due to the barrier must be compensated by a reduction in d. The energy increase of the system would be at its greatest when the skyrmions are in the middle of the barrier; hence the biggest deflection is seen at this point. Due to this quick adjustment of d, the skyrmions speed up as they traverse the barrier.

Another interesting feature of the scattering on a barrier is the 'transition dynamics' shown in figure 5. These plots show the transition to a state in which the skyrmions do not traverse the barrier and, instead, move away from each other. The transition to such a state is shown through the variation in the potential coefficient Γ for a fixed value of the barrier width $b = 3$. Similar plots could also have been obtained by choosing a fixed value of $\Gamma \simeq 0.25$ and increasing the barrier width b from $b = 2$ to $b = 3$. This effect is due to the binding energies of the skyrmion configuration. Using the previous definition of the binding energy (24) and its constituent parts, one can examine the binding energies in the barrier system. In a system with $b = 2$ and $\Gamma = 0.1$, $E_2 = 2.1317/8\pi$ and $E_1 = 1.0723/8\pi$; therefore, $E_B = -0.0087/8\pi$ so the skyrmions are still bound. In $b = 2$ and $\Gamma = 0.3$, $E_2 = 2.1397/8\pi$ and $E_1 = 1.0730/8\pi$; therefore, $E_B = -0.0063/8\pi$ and the skyrmions are still bound although a bit more loosely than for the smaller value of Γ. Next, consider the state where the skyrmions separate from each other, i.e. for $b = 3$ and $\Gamma = 0.25$. Then $E_2 = 2.1482/8\pi$ and $E_1 = 1.0767/8\pi$ and, therefore, $E_B = -0.0052/8\pi$. The trajectory clearly shows that the skyrmions, for these values of b and Γ, behave as if they are unbound. Thus, there appears to exist a threshold value of E_B in the barrier system, according to our definition of E_B, which determines whether the skyrmions are bound or unbound. This threshold value is b dependent, but is approximately around $E_B = -0.005/8\pi$. We believe that this threshold is associated with the 'tails' of the skyrmions.

When two skyrmions are well separated, they interact through their tails. In the new baby-skyrme model, the skyrmions are exponentially localized. Examining the limit of the differential equation (19) describing the profile function $f(r)$, for large r, the exponential

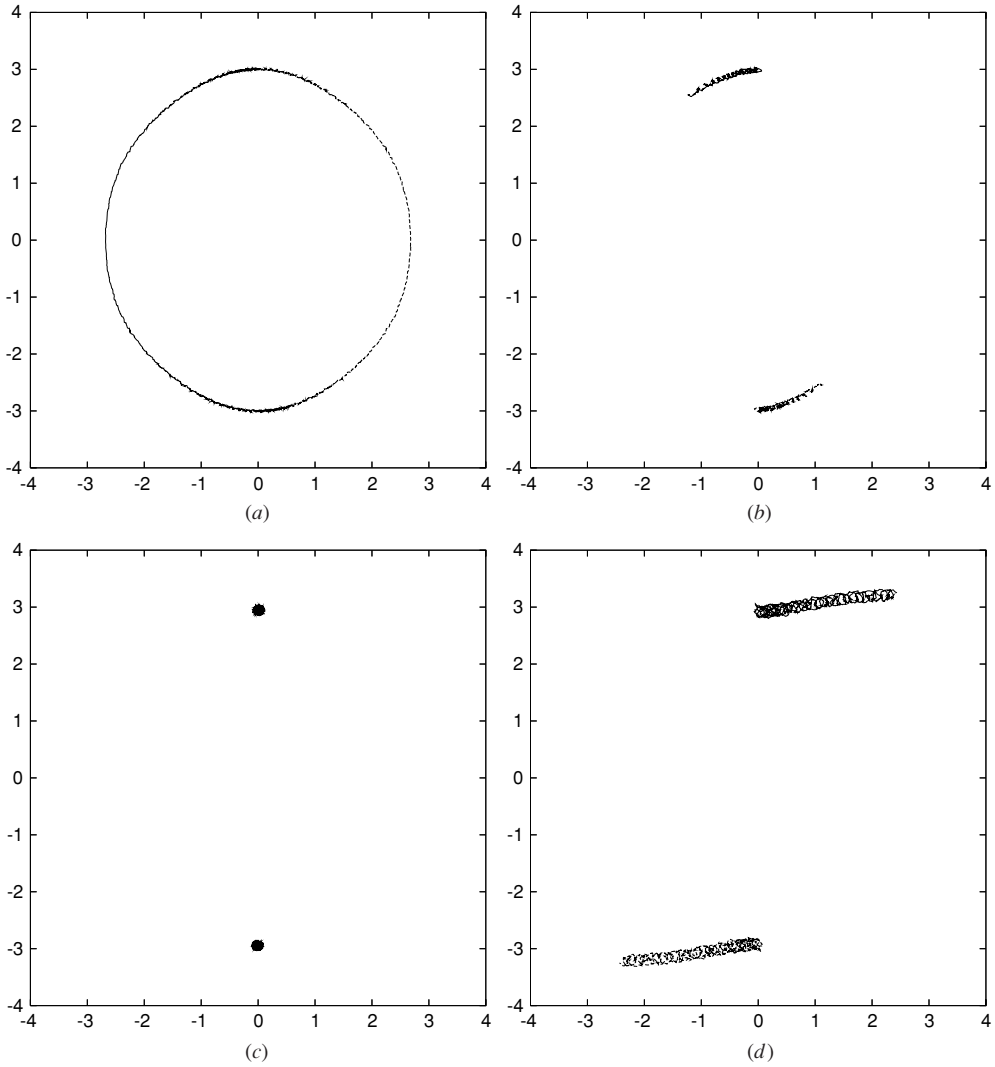

Figure 5. Plots showing the transition to asymptotic state $b = 3$ $\Gamma = 0.25$, through variations in Γ for a fixed $b = 3$: (*a*) $\Gamma = 0.10$, (*b*) $\Gamma = 0.15$, (*c*) $\Gamma = 0.20$ and (*d*) $\Gamma = 0.25$.

localization is evident. The solution to these differential equations is the modified Bessel functions

$$f(r) \sim \frac{1}{\sqrt{\gamma_3 r}} \exp(-\gamma_3 r). \tag{25}$$

The localization of the profile function for a skyrmion is governed by the potential term coefficient γ_3. The potential obstructions were introduced as inhomogeneities, in the space of the potential coefficient, γ_3 s value. In the barrier system, the potential coefficient γ_3 takes the value of $\gamma_3 + \Gamma$ on the barrier. There, the asymptotic value of the profile function is modified:

$$\gamma_3 \to \gamma_3 + \Gamma, \tag{26}$$

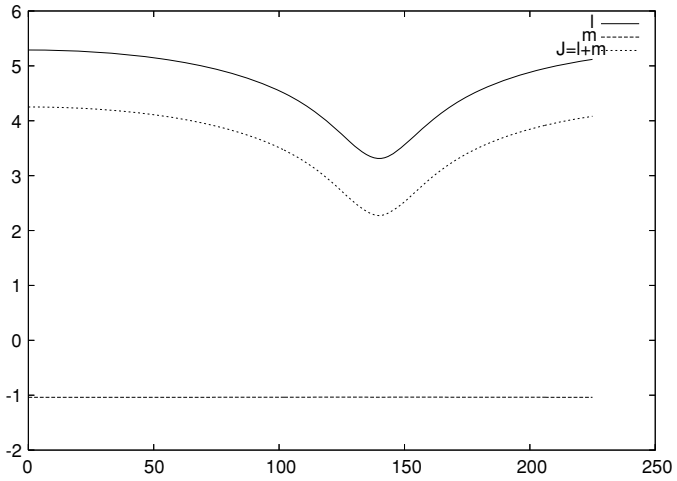

Figure 6. Plots of the orbital angular momentum l, total magnetization m and total angular momentum $J = l + m$ for $b = 2$, $\Gamma = 0.25$.

$$f(r) \sim \frac{1}{\sqrt{(\gamma_3 + \Gamma)r}} \exp(-(\gamma_3 + \Gamma)r).$$

As the skyrmion tail penetrates the region, it becomes attenuated by the potential obstruction. The width of the barrier causes the tail to be attenuated earlier for a larger value of b than for a smaller one. If, as we have assumed, the appreciable interaction of two well-separated skyrmions is due to the tail–tail interaction between them, then if these tails are attenuated, the interaction must also be reduced. Thus, there must exist a value of Γ, the size of the attenuation of the tail in the obstruction, for which the appreciable interaction of the skyrmions' tail is no longer sufficient for the skyrmions to undergo their usual dynamics. If there exists a critical value for Γ, then there must exist a critical value of E_B. Thus the threshold value of the binding energy corresponds to the particular values of b and Γ for which the tail–tail interaction of the skyrmions is no longer sufficient to cause the usual circular motion, and the skyrmions can separate off from each other.

6. Angular momentum

In this section we present the explanation of our results based on the study of the total angular momentum J. The orbital angular momentum l and the total magnetization in the third direction m were calculated through all the simulations using the definitions given by (1) and (7). Figure 6 shows a plot of l, m and J for a two 1-skyrmion configuration interacting with a potential barrier of width $b = 2$ and $\Gamma = 0.25$. It is clear that $\dot{m} = 0$ throughout, but that l and J are not conserved in time.

In systems involving a two 1-skyrmion configuration the guiding centre coordinate $\underline{R}$, defined in (14), corresponds to the centre of the configuration. A calculation of $\underline{R}$ during the barrier simulations has indeed shown that $\underline{R} = 0$. This is expected since the trajectories of the skyrmions in the system are always symmetric with respect to a reflection through the origin and so the centre of the configuration always lies at this point. Considering (15) with $\underline{R} = 0$,

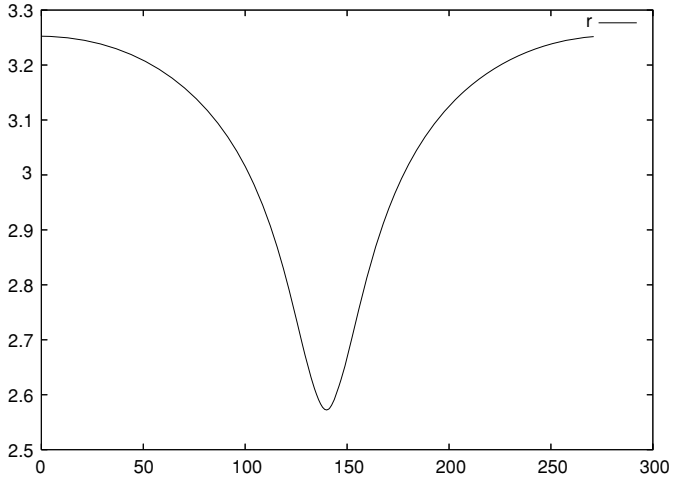

Figure 7. Plot of the average skyrmion radius as a function of time for a potential barrier with $b = 2$ and $\Gamma = 0.25$.

we note that the orbital angular momentum l and the average size of the skyrmions r are now directly related to each other in the barrier system by

$$r^2 = \frac{l}{2\pi Q}. \tag{27}$$

Figure 7 shows a plot of the average skyrmion radius as a function of time for a potential barrier system of width $b = 2$ and $\Gamma = 0.25$. The points at which $r(t)$ approaches its minimum corresponds to the skyrmions traversing the barrier. The point at which they have reached the maximum of the barrier corresponds to the minimum of $r(t)$. Thus as the skyrmions traverse the barrier, their average size decreases from its starting value by around 20%. Since the tail of the skyrmion is exponentially localized and this localization is governed by the potential coefficient parameter γ_3, it is expected that due to the inhomogenaity in γ_3 their size would decrease in the region of larger γ_3 explaining the observed behaviour in l.

Figure 8 shows a plot of l, m and J for a two 1-skyrmion configuration interacting with a potential hole of width $b = 2$ and $\Gamma = 0.25$. Again, it is clear that $\dot{m} = 0$ throughout, but l and J are not conserved in time, analogous to what was seen in the system involving a potential barrier. The guiding centre coordinate $\underline{R}$ for this system can also be shown to vanish and thus (14) is valid also in systems with potential holes. Using this, we can therefore plot $r(t)$ for a potential hole. Figure 9 shows a plot of the average skyrmion radius as a function of time for a potential hole system of width $b = 2$ and $\Gamma = -0.25$. It is clear from the plot that as the skyrmions approach the boundary asymptotically along the edge of the hole, the average size of the skyrmion increases continually, increasing to approximately thrice its initial size. This is due to the tail of the skyrmions. The skyrmions cannot penetrate the hole, as explained in the previous sections, but their tail can. The exponential localization of the skyrmions, as explained earlier, is governed by the potential coefficient γ_3. In the region of reduced γ_3, their average size is able to grow and so it continues to increase until they reach the boundary of the system where they get reflected. In our simulations we saw that following this reflection the skyrmions' size decreases back to its starting value as the system tends to its starting point.

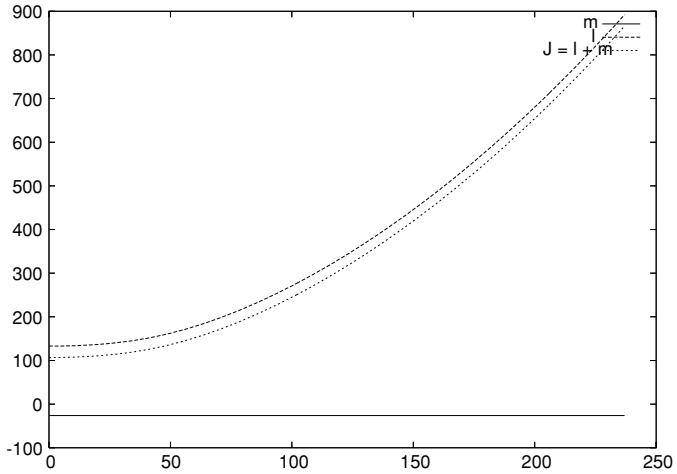

Figure 8. Plots of the orbital angular momentum l, total magnetization m and total angular momentum $J = l + m$ for a potential hole with $b = 2\ \Gamma = -0.25$.

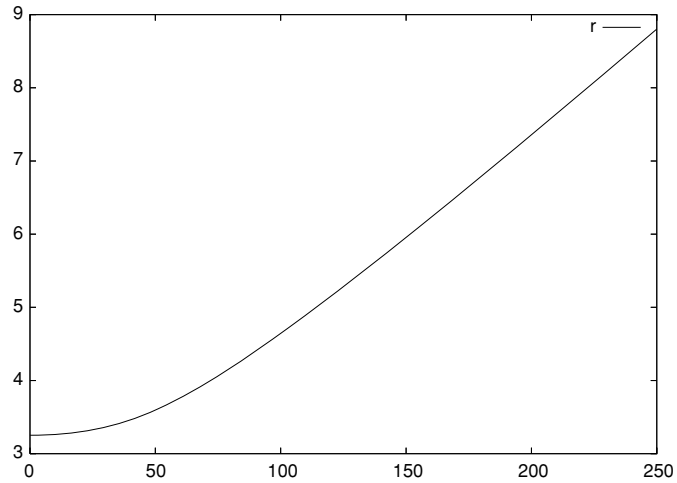

Figure 9. Plot of the average skyrmion radius as a function of time for a potential hole with $b = 2$ and $\Gamma = -0.25$.

7. Further discussion of angular momentum

Here we discuss further the apparent non-conservation of J. Assuming the definitions of l, m and hence of J to be valid and shown to be true in the free system, we ask ourselves: can we explain this more qualitatively? Let us consider the behaviour of J. The form of $l(t)$ from figure 6 indicates that $\dot{l} \neq 0$ and hence $\dot{J} \neq 0$. The calculation of l includes only the contribution of the fields, but clearly this may, for systems involving obstructions, not be sufficient. We can consider adding an external contribution due to the potential obstruction and see whether this restores J-conservation. How the potential obstructions affect, if at all, the orbital angular momentum needs to be considered. The symmetric obstructions can be

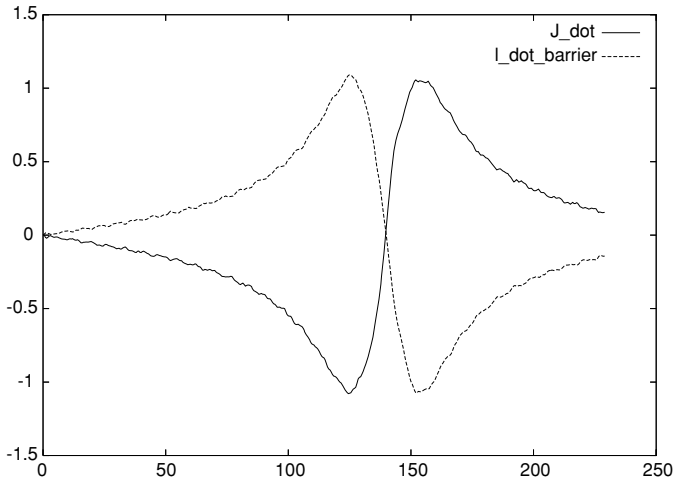

Figure 10. Plots of the numerically calculated time derivative of the total angular momentum $J = l + m$ and the contribution of the barrier to $\dot{l}$ for $b = 2\ \Gamma = 0.25$.

written as a contribution to the potential term $V(\phi)$ in terms of the Heaviside functions. The potential term and this inhomogeneity expressed in terms of the Heaviside functions can be written as

$$V(\phi) = \tfrac{1}{2}\gamma_3\left(1-\phi_3^2\right) \pm \tfrac{1}{2}\Gamma\left(1-\phi_3^2\right)\left[\Theta(y+y_0) - \Theta(y-y_0)\right]. \tag{28}$$

Using the above definition of $V(\phi)$, one can compute the contribution made to $\dot{l}$ in addition to the fields already computed from (1). One needs to construct $\dot{q}$ from its constituent parts as shown in (9):

$$\dot{q} = -\epsilon_{ij}\partial_i\partial_l\sigma_{jl} = -\epsilon_{ij}\partial_i\left(\frac{\delta W}{\delta \underline{\phi}}\cdot\partial_j\underline{\phi}\right).$$

Using the properties of the Heaviside functions and their relations to the δ-function one can show that the potential obstruction's contribution to $\dot{q}$ is given by

$$\dot{q} = \pm\phi_3\partial_x\phi_3\Gamma\left[\delta(y+y_0) - \delta(y-y_0))\right].$$

With this expression for $\dot{q}$, we can evaluate the total rate of change of the orbital angular momentum due to the obstruction. We find

$$\begin{aligned}\dot{l} &= \frac{1}{2}\int\!\!\int_{-\infty}^{\infty}(x^2+y^2)\dot{q}\,\mathrm{d}x\,\mathrm{d}y \\ &= \frac{\pm\Gamma}{2}\int_{-\infty}^{\infty}\mathrm{d}x\int_{-\infty}^{\infty}(x^2+y^2)\partial_x\left(\frac{1}{2}\phi_3^2\right)\left[\delta(y+y_0)-\delta(y-y_0))\right]\mathrm{d}y \\ &= \frac{\pm\Gamma}{2}\int_{-\infty}^{\infty}\mathrm{d}x(x^2+y^2)\partial_x\left(\frac{1}{2}\phi_3^2\right)\Bigg|_{y=y_0}^{y=-y_0}.\end{aligned} \tag{29}$$

The integrals in (29) have been calculated during each simulation. Figure 10 shows the numerically computed integral contributions due to the obstruction and the numerically calculated derivative of the orbital angular momentum from figure 6 plotted with respect to time, for a potential barrier with $b = 2$ and $\Gamma = 0.25$. It can be seen from the plot that the

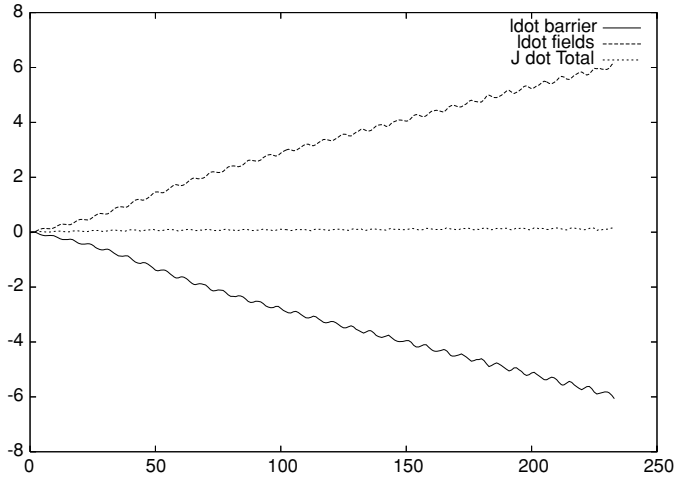

Figure 11. Plots of the numerically calculated time derivative of the total angular momentum $J = l + m$ for the fields and the contribution of the hole to $\dot{l}$ for $b = 2$ $\Gamma = -0.25$.

time evolution of the integral contributions exactly matches that of $\dot{l}$ due to the fields, so that we have

$$\dot{l} = \dot{l}_{\text{fields}} + \dot{l}_{\text{barrier}} \tag{30}$$

$$= \frac{\mathrm{d}}{\mathrm{d}t}\left[\frac{1}{2}\int\int_{-\infty}^{\infty}(x^2+y^2)q\,\mathrm{d}x\,\mathrm{d}y\right] + \frac{\pm\Gamma}{2}\int_{-\infty}^{\infty}\mathrm{d}x(x^2+y^2)\partial_x\left(\frac{1}{2}\phi_3^2\right)\Big|_{y=y_0}^{y=-y_0} \tag{31}$$

$$\simeq 0. \tag{32}$$

Due to discretization effects and numerical inaccuracies, the result is not exact but the qualitative features of the integral contributions make this a very consistent result.

Figure 11 shows the numerically computed integral contributions due to the obstruction and the numerically calculated derivative of the orbital angular momentum from figure 8 plotted with time, for a potential hole with $b = 2$ and $\Gamma = 0.25$. It is clear from these plots that the conservation of the total angular momentum J is restored by the introduction of the terms corresponding to the potential obstructions' contribution to $\dot{l}$.

8. Conclusions

Our studies have shown that the scattering of baby skyrmions of our model off potential obstructions, for which the dynamics is governed by the Landau–Lifshitz equation, exhibits some nontrivial results.

We have managed to understand quite well the observed scattering properties of our skyrmions despite their, at first sight, somewhat non-intuitive behaviour. Thus, in the case of a potential hole the skyrmions were unable to penetrate it and so moved parallel to the x-axis at a distance y^s_{max} from the hole. The energy considerations have shown that the skyrmions, in systems involving a potential hole, became unbound as they approached the hole and so could and did move away from each other.

In the barrier systems the skyrmions were able to traverse the barrier. Our simulations have shown that as the skyrmions traversed the barrier their distance of separation d decreased

to overcome this increase in potential energy. At the same time the skyrmions sped up as they climbed the barrier. The transition dynamics has showed that there exists a threshold value of the binding energy in the barrier systems $E_B \simeq -0.005/8\pi$. By comparison, in the absence of any potential obstructions, the binding energy of the two skyrmions is $E_B = -0.11/8\pi$. So this threshold binding energy is roughly half the binding energy if there was no barrier. Above this value the skyrmions behave as a bound state, and below which they can separate from each other. Our intuition and reasoning have led us to the conclusion that the tail–tail interaction between the skyrmions is reduced due to the attenuation of the skyrmion tail by the barrier, and this is responsible for this 'threshold' effect.

An interesting observation of our simulations was the apparent non-conservation of the total angular momentum J (given its usual definition). This non-conservation of J was due to the non-conservation of the orbital angular momentum l, as we have found that in all of the simulations the total magnetization in the third direction m was well conserved in time. At the same time we showed that $\dot{l} \neq 0$. Thinking about this further we showed that when a system possesses potential obstructions, these obstructions made a significant contribution to $\dot{l}$. Hence one has to modify the conventional definition of l. We have found this missing contribution and we have shown that its change compensates $\dot{l}$, resulting in the overall conservation of l and J for the full system. We believe that most of the results presented here form a generic basis for the description of the scattering of baby-skyrmion configurations in the Landau–Lifshitz models. This is primarily due to conservation laws of the Landau–Lifshitz systems, as constructed by Papanicolaou and Tomaras [10], and the observation that the potential obstructions contribute to the conservation laws of the system.

References

[1] Brand J, Piette B and Zakrzewski W 2005 Scattering of topological solitons on holes and barriers *J. Phys. A: Math. Gen.* **38** 10403–12
[2] Speight J M 2006 Sigma models on curved space and bubble refraction in doped antiferromagnets *Nonlinearity* **19** 1565–79
[3] Bobeck A H and Della Torre 1975 *Magnetic Bubbles (Selected Topics in Solid State Physics)* (Amsterdam: North-Holland)
[4] O'Dell T H 1974 *Magnetic Bubbles* (London: Macmillan)
[5] Derrick G H 1964 Comments on nonlinear wave equations as models for elementary particles *J. Math. Phys.* **5** 1252
[6] Weidig T 1999 The baby Skyrme models and their multi-skyrmions *Nonlinearity* **12** 1489–503
[7] Papanicolaou N and Zakrzewski W 1996 Dynamics of magnetic bubbles in skyrme model *Phys. Lett.* A **210** 328–36
[8] Papanicolaou N and Zakrzewski W 1995 Dynamics of interacting magnetic vortices in a model Landau–Lifshitz equation *Physica* D **80** 225–45
[9] Eslami P, Sarbishaei M and Zakrzewski W 2000 Baby Skyrme models for a class of potentials *Nonlinearity* **13** 1867–81
[10] Papanicolaou N and Tomaras T N 1991 Dynamics of magnetic vortices *Nucl. Phys.* B **360** 425–62